2D Homogeneous Turbulence

2D homogeneous turbulence is relevant to geophysical turbulence on large horizontal scales because of the thinness of Earth's atmosphere and ocean (*i.e.,* $H/L \ll 1$) and Earth's rotation (*i.e.,* $Ro \ll 1$) and stable stratification (*i.e.,* $Fr \ll 1$), both of which tend to suppress vertical flow and make the 2D horizontal velocity component dominant. A detailed explanation for this involves the theory for geostrophic turbulence, which is a later topic. Danilov and Gurarie (2000) is a review of the connection between 2D and geostrophic turbulence.

The homogeneous momentum and continuity equations are also applicable to 2D flow. Its vectors are, of course, 2D, and we will identify these two dimensions with the horizontal coordinates (x, y) and velocities (u, v). Thus, $w = \partial_z = 0$. Because of horizontal non-divergence,

$$\mathbf{u} \;=\; \hat{\mathbf{z}} \times \nabla\psi \;, \tag{1}$$

and the only vorticity component is vertical, $\vec{\zeta} \;=\; \hat{\mathbf{z}}\zeta$, with

$$\zeta \;=\; \nabla^2\psi \;. \tag{2}$$

The vorticity equation is particularly simple in 2D flows,

$$\frac{D\zeta}{Dt} \;=\; \nu\nabla^2\zeta \;, \tag{3}$$

lacking any vortex stretching. It is isomorphic to a passive scalar equation, but it also governs the flow evolution through (1)-(2). Thus, vorticity extrema can only decay with time, but the decay can be slow if viscous effects are weak and a forward cascade is not efficient (as occurs locally inside 2D coherent vortices when $Re \gg 1$; Sec. 2).

2D flow fits into the special category of horizontally non-divergent horizontal flows discussed in *Turbulent Flows: General Properties* — except here without any z dependence in ψ. There an analysis is made the local gradient advective competition between dominance by vorticity or strain rate, *i.e.,* coherence or cascade. This analysis is perhaps the most fundamental one for 2D turbulence, playing an analogous role in this regard to the Kolmogorov cascade analysis for 3D turbulence, whose local evolutionary process is primarily by vortex stretching. A clear difference between these two conceptual views is that there is a non-cascading component in 2D turbulence (*i.e.,* quantities whose spectrum variance does not systematically move in wavenumber space towards either larger or smaller wavenumbers and whose patterns are persistent rather than evanescent). Insofar as 2D turbulence is a dynamical paradigm for turbulence in highly anisotropic flows — as occur in many geophysical regimes — then the latter too will have non-cascading components. There are no 2D flows in nature, although there are rather strong approximate isomorphisms with the dynamics in non-neutral plasmas and thin soap films, which have therefore provided at least a limited laboratory experimental comparison standard for 2D theory and modeling; hence, the primary evidence has come from computations; these are all the more feasible in 2D at large Re because there is one fewer space dimension to span than in 3D. So, the basis of our interest in 2D turbulence is as a possible paradigm for anisotropic turbulence, not its physical realizability. Its great virtue as a dynamical system for turbulence is its greater computability because of its lower spatial dimensionality.

Unlike the unsolved proof or disproof of global regularity in the 3D Navier-Stokes equations, the matter in 2D has long been resolved in favor of regularity (Lions and Prodi, 1959; Ladyzhenskaya, 1969).

1 Energy and Enstrophy Cascades

Turbulence is an inherently dissipative phenomenon since advectively induced cascades spread the variance across different spatial scales, reaching down to arbitrarily small scales where molecular viscosity and diffusion can dampen the fluctuations through mixing. Integral kinetic energy and *enstrophy* (*i.e.,* vorticity variance) budgets can be derived from the momentum equations with spatially periodic boundary conditions (for simplicity):

$$\begin{aligned} \frac{dE}{dt} &= -\nu \int\int dx\, dy\, (\nabla \mathbf{u})^2 \;=\; -\mathcal{E} \\ \frac{d\,Ens}{dt} &= -\nu \int\int dx\, dy\, (\nabla \zeta)^2 \;=\; -\int\int dx\, dy\, \hat{\eta}\,, \end{aligned} \tag{4}$$

where

$$E \;=\; \frac{1}{2}\int\int dx\, dy\, \mathbf{u}^2\,, \tag{5}$$

and

$$Ens \;=\; \frac{1}{2}\int\int dx\, dy\, \zeta^2\,. \tag{6}$$

(In *Turbulent Flows*, $\int\, \hat{\eta}\, d\mathbf{x}$ was denoted as $\mathcal{E}_\zeta$ at the end of Sec. 1.) Therefore, due to the viscosity, E and Ens are non-negative quantities that are non-increasing with time as long as there is no external forcing of the flow. The respective dissipation rates are ε and $\hat{\eta}$ (not to be confused with the Kolmogorov scale in 3D).

The common means of representing the scale distribution of a field is through its Fourier transform and spectrum. For example, the Fourier transform of $\psi(\mathbf{x})$ is $\hat{\psi}(\mathbf{k})$, and its spectrum is $S(\mathbf{k}) \;=\; \langle\, |\hat{\psi}(\mathbf{k})|^2 \,\rangle$. The averaging is over any appropriate symmetries for the physical situation of interest (*e.g.,* over time in a statistically stationary situation, over the directional orientation of $\mathbf{k}$ in an isotropic situation, or over independent realizations in a recurrent situation). $S(k)$ can be interpreted as the variance of ψ associated with a spatial scale, $L = 1/k$, with $k = |\mathbf{k}|$, such that the total variance, $\int d\mathbf{x}\psi^2$, is equal to $\int\, d\mathbf{k}\, S$ (*i.e.,* Parceval's Theorem).

With a Fourier representation, the energy and enstrophy are integrals over their corresponding spectra,

$$E \;=\; \int\, d\mathbf{k}\, E(\mathbf{k}), \quad Ens \;=\; \int\, d\mathbf{k}\, Ens(\mathbf{k})\,, \tag{7}$$

with

$$E(\mathbf{k}) \;=\; \frac{1}{2}k^2\, S, \quad Ens(\mathbf{k}) \;=\; \frac{1}{2}k^4\, S \;=\; k^2\, E(\mathbf{k})\,. \tag{8}$$

In the latter relations, the spatial gradient of ψ has a Fourier transform equal to the product of $i\mathbf{k}$ and $\hat{\psi}$. In an isotropic flow the spectrum is a function only of k, not $\mathbf{k}$, even though the transform itself $\hat{\psi}$ remains a function of $\mathbf{k}$ at any given time (*i.e.,* it contains spatial phase information about the pattern). The spectra in (8) have different shapes due to their different weighting factors of k, and the enstrophy spectrum has a relatively larger magnitude at smaller scales (larger k) than does the energy spectrum (Fig. 1, top).

In the absence of viscosity — or during the early time in the interval after initialization with smooth, large-scale fields before the cascade carries enough variance to small scales to make the

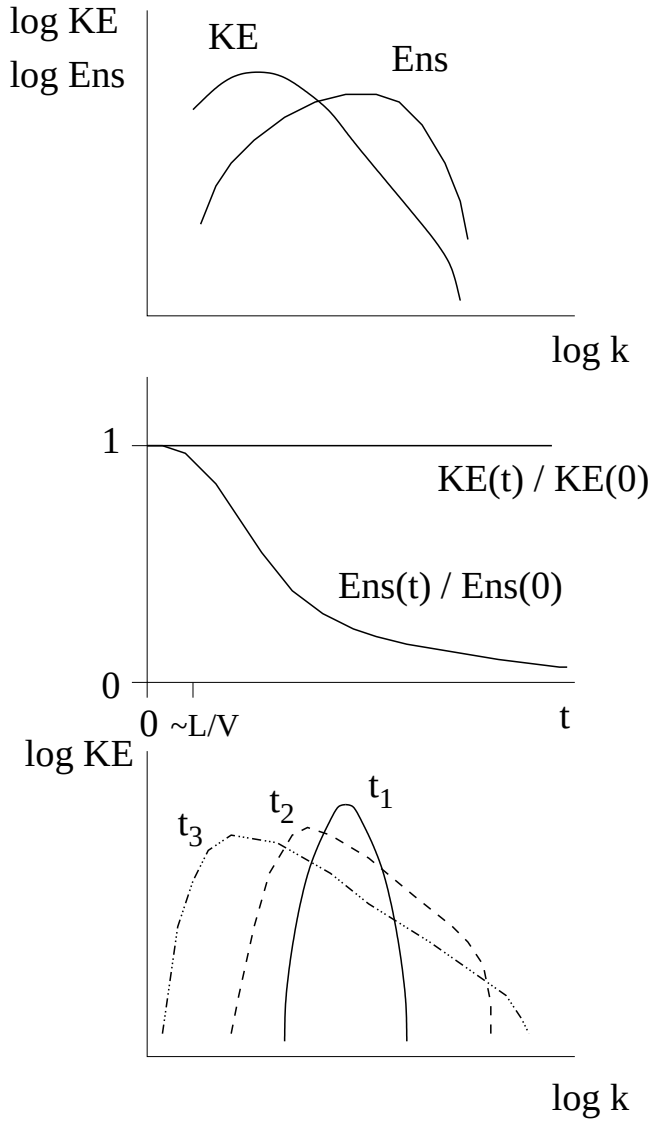

Figure 1: (Top) Schematic isotropic spectra for energy $E(k)$ and enstrophy $Ens(k)$ in 2D turbulence at large Reynolds number. Note that the energy peak occurs at smaller k than the enstrophy peak. (Middle) Time evolution of total energy $E(t)$ and enstrophy $Ens(t)$, each normalized by their initial value. The energy is approximately conserved when $Re \gg 1$, but the enstrophy has significant decay over many eddy advective times L/V. (Bottom) Evolution of the energy spectrum $E(k,t)$ at three successive times, $t_1 < t_2 < t_3$. With time the spectrum spreads, and the peak moves to smaller k.

right-side terms in (4) significant — both E and Ens are conserved with time. If the cascade process broadens the spectra (a generic behavior in turbulence, transferring variance across different spatial scales), the only way that both integral quantities can be conserved, given their different k weights, is that more of the energy is transferred toward larger scales (smaller k) while more of the enstrophy is transferred toward smaller scales (larger k). This behavior is firmly established by computational and laboratory studies, and it can, at least partly, be derived as a necessary consequence of spectrum broadening by the cascades. Define a *centroid wavenumber* k_E (*i.e.,* a characteristic wavenumber averaged across the spectrum), and a *wavenumber bandwidth* Δk_E for the energy spectrum as follows:

$$\begin{aligned} k_E &= \int d\mathbf{k}\,|\mathbf{k}|\,E(\mathbf{k}) \Big/ E \\ \Delta k_E &= \left(\int d\mathbf{k}\,(|\mathbf{k}| - k_E)^2\,E(\mathbf{k}) \Big/ E \right)^{1/2} . \end{aligned} \tag{9}$$

Both quantities are positive by construction. If the turbulent evolution broadens the spectrum, then conservation of E and Ens (*i.e.,* $\dot{E} = \dot{Ens} = 0$, with the overlying dot again denoting a time derivative) implies that the energy centroid wavenumber must decrease,

$$\dot{\Delta k}_E > 0 \quad \Rightarrow\ -2k_E\dot{k}_E > 0 \quad \Rightarrow\ \dot{k}_E < 0\,.$$

This implies a systematic transfer of the energy toward larger scales. This tendency is accompanied by an increasing enstrophy centroid wavenumber, $\dot{k}_{Ens} > 0$ (with k_{Ens} defined analogously to k_E).[1] These two, co-existing tendencies are referred to, respectively, as the *inverse energy cascade* and the *forward enstrophy cascade* of 2D turbulence. The indicated direction in the latter case is "forward" to small scales and large k values, which is the most common behavior for different quantities in different regimes of turbulence (*e.g.,* in 3D, uniform-density turbulence, the energy cascade is in the forward direction, and while Ens is not an inviscid integral invariant, its cascade direction is also forward).

In the presence of viscosity — or after the forward enstrophy cascade acts for long enough to make the dissipation terms become significant — E will be much less efficiently dissipated than Ens because so much less of its variance — and the variance of the integrand in its dissipative term in the right side of (4) — resides in the small scales. Thus, for large Re (small ν), Ens will decay significantly with time while E may not decay much at all (Figs. 1, middle, and 2)[2]. Over the course of time, the energy spectrum shifts toward smaller wavenumbers and larger scales due to the inverse cascade, and its dissipation rate further declines (Fig. 1, bottom).

From the above, it is therefore plausible that, as $Re \to \infty$, $\mathcal{E} \to 0$, and $\mathcal{E}_\zeta$ approaches a finite value at least after the interval of spectrum broadening extends the enstrophy spectrum to the viscous scales. It is the enstrophy dissipation that is of central important in 2D turbulence, in contrast to the energy dissipation in 3D (*n.b.,* hypothesis H3 in *3D Homogeneous Turbulence*). We can make a scaling estimate for the enstrophy dissipation rate $\hat{\eta}$:

$$\hat{\eta} \;=\; \frac{Ens}{\tau_\zeta} \;=\; Ens^{3/2}, \tag{10}$$

[1] The only proof this statement is too lengthy to include here.

[2] In decaying 3D turbulence, energy is efficiently dissipated through its forward cascade, with $E \propto t^{-1}$ (Batchelor, 1953).

where the the nonlinear evolutionary time scale is an advective one, like the eddy turnover time, but associated with the enstrophy, $\tau_\zeta = Ens^{-1/2}$, whose spectrum peak is at smaller scales (Fig. 1, top). The necessary time interval to reach the dissipation scales from smooth initial conditions is $t - t_0 \sim \tau_d = L_o/V_o \log Re$ (as seen from closure-theory calculations (*e.g.,* Lesieur, 1997) and numerical solutions). This time formally $\to \infty$ as $Re \to \infty$ — in contrast with the 3D cascade where the time of onset of dissipation is finite as $Re \to \infty$; see the previous predictability discussion — but its logarithmic dependence is so weak that in practice this time is only a few large-eddy turnover times L_o/V_o. Note that both $1/\tau_\zeta$ and $\hat{\eta}$ will decrease with time if Ens is not renewed against dissipation, and the energy-related advective rate V_o/L_o will also decrease if $L_o \sim 1/k_e$ grows while $V_o \sim E^{1/2}$ is preserved by the inverse cascade. Also note that τ_d can also be expressed as

$$\tau_d \;=\; Ens^{-1/2} \log Re \tag{11}$$

for the early-time evolution from narrow-band initial conditions, since the energy and enstrophy time scales are identical then.

Because $\mathcal{E} \to 0$ as $Re \to \infty$, E is referred to as a *rugged invariant* in 2D turbulence, because (as with the circulation or total material content in either 2D or 3D) it has the same conservative behavior with small ν, κ as with zero ν, κ. Obviously, Ens — like the scalar variance V (*Turbulent Flows*, eq. (4)) in either 2D or 3D — is not a rugged invariant. Most conservative invariants of Euler equations are not rugged invariants in most regimes of turbulence, but the few that are rugged ones are very important as interpretive constraints on the evolution.

2 Decaying 2D Turbulence and Coherent Vortex Emergence

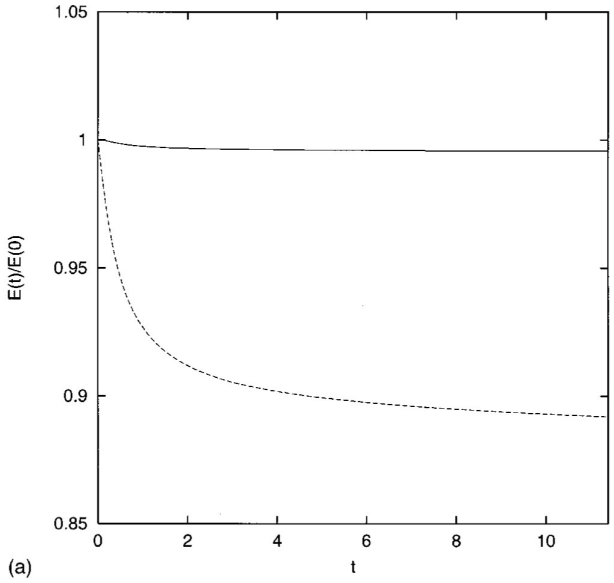

Figure 2: Kinetic energy in decaying 2D turbulence, normalized by the initial energy and an eddy turnover time. The dashed curve has a much lower Re value than the solid curve, and their forcings are at large and small scales, L_{f1} and L_{f2} respectively. (Bracco *et al.*, 2000)

The cascade and dissipation in 2D turbulence co-exist with vortex emergence, movement, and mergers (Fig. 3). From smooth initial conditions, coherent vortices emerge by *axisymmetrization*; move approximately the same way *point vortices* do; they occasionally *couple* as rapidly moving dipole vortex pairs for brief intervals; and they *merge* when two with the same circulation parity move close enough together (Fig. 4)[3]. (These vortex processes are described further in the Appendix.) With time there are fewer vortices become fewer; they are larger, and sparser in space, and they undergo less frequent close encounters. Since those close encounters are the occasions when the vortices change through deformation in ways other than simple movement, the overall evolutionary rates for the spectrum shape and vortex population become ever slower, even though the kinetic energy does not diminish. Enstrophy dissipation occurs primarily during emergence and merger events, as *filaments* of vorticity are stripped off of vortices. The filamentation is a consequence of the differential velocity field (*i.e.,* shear, strain rate) of one vortex acting on another; this increases rapidly as the vortex separation distance diminishes. The filaments continue irreversibly to elongate until their transverse scale shrinks enough to come under the control of viscous diffusion, and the enstrophy they contain is thereby dissipated. So, the integral statistical outcomes of cascade and dissipation in 2D turbulence are the result of a local dynamical processes sequence of the elemental coherent vortices, at least during the period after their emergence from complex initial conditions or forcing. The vortices substantially control the dynamics of 2D turbulent evolution.

The preceding discussion refers to freely evolving or *decaying* turbulence, where the ultimate outcome is energy and enstrophy dissipation through the inexorable action of viscosity. Alternatively, one can consider forced, *equilibrium* turbulence, where a statistically stationary state occurs with the turbulent generation rate balancing the dissipation rate for energy, enstrophy, and all other statistical measures. The generation process may either be the instability of a forced mean flow or be an imposed fluctuating force. For 2D turbulence with fluctuations generated on intermediate spatial scales (smaller than the domain size and larger than the viscous scale), inverse energy and forward enstrophy cascades ensue (Sec. 4). To achieve an equilibrium energy balance some dissipative process, beyond viscosity, must be included to deplete the energy at large scales, or else this component of the energy will continue to grow through its inverse cascade. (A common choice is a linear drag force, motivated by the effect of an Ekman boundary layer.) The degree of coherent vortex emergence and subsequent dynamical control of the equilibrium turbulence depends upon the relative rates of forcing and energy dissipation (which disrupt the vortex dynamics) and of vortex advection (which sustains it).

Now we consider the continuation of the initial-value problem, going beyond the early phase of spectrum broadening through the dual cascades, inverse in energy and forward in enstrophy. We assume that the domain size is large compared to the scale of the initial conditions k_o^{-1} and that the boundary conditions are periodic in both x and y; periodicity requires that $\int\int \zeta \, \mathbf{dx} = 0$ so that $\nabla^2 \psi = \zeta$ has a solution for ψ. The time histories of the kinetic energy and its wavenumber spectrum are shown in Figs. 2-5. At early times, for $t < \tau_d$, the plotted statistical measures are essentially unchanged from their initial values, except for the spectrum centroid wavenumbers which change in the expected sense, $\dot{k}_e < 0$ and $\dot{k}_{ens} > 0$. Once the spectrum has broadened to reach the dissipation wavenumber k_d (22), then the enstrophy dissipation rate $\hat{\eta}$ begins to grow and the enstrophy, Ens, begins to decay; in contrast, the energy E hardly decays at all, although

[3]Note that the 2D merger process is the topologically equivalent to the parallel vortex reconnection process in 3D.

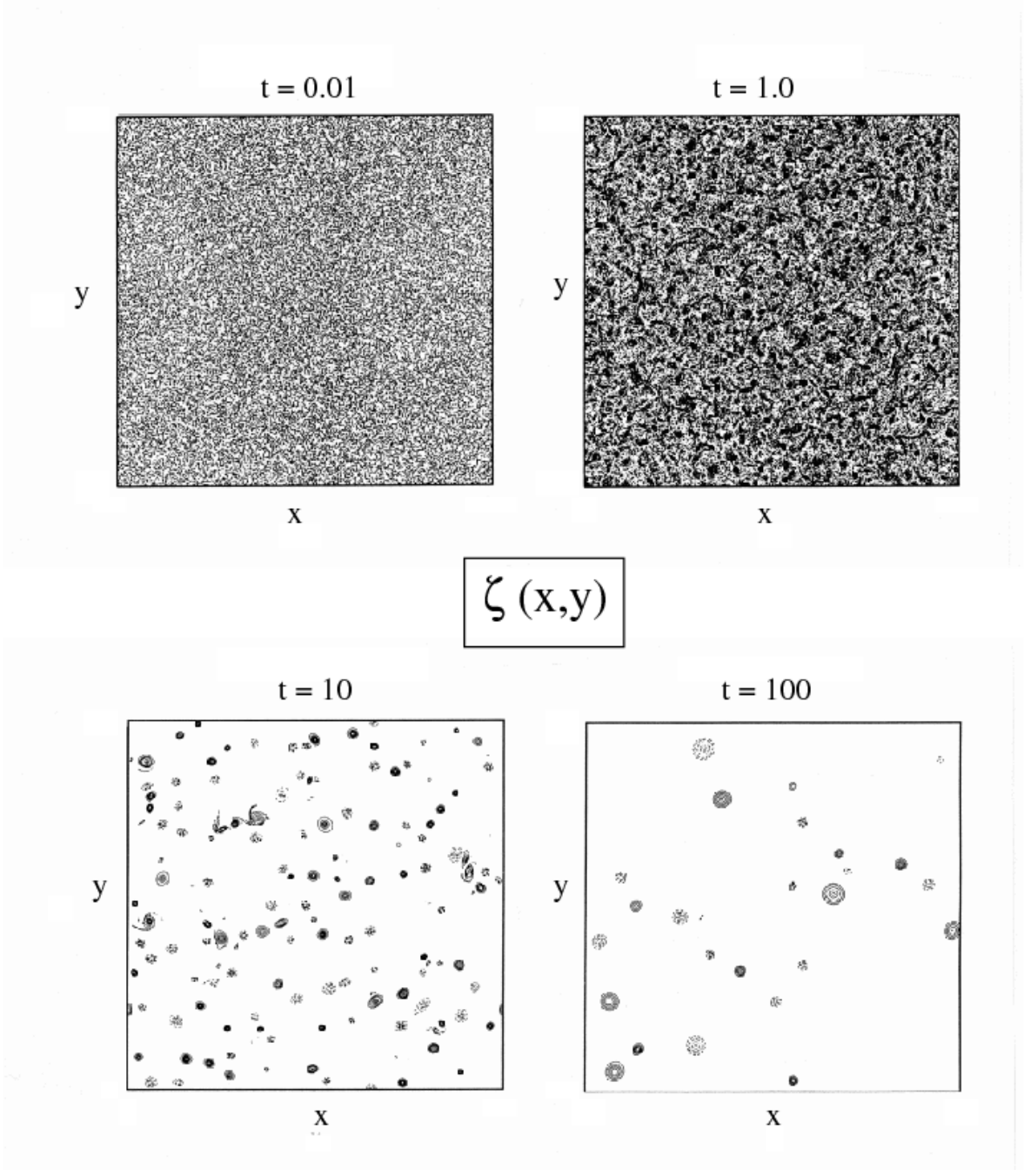

Figure 3: Vortex emergence and evolution in computational 2D turbulence, as seen in $\zeta(x, y)$ at sequential times, with random, spatially smooth initial conditions. Solid contours are for positive ζ, and dashed ones are for negative ζ. The contour interval is twice as large in the first panel as in the others. The times are non-dimensional based on an advective scaling L/V. (Adapted from McWilliams, 1984.)

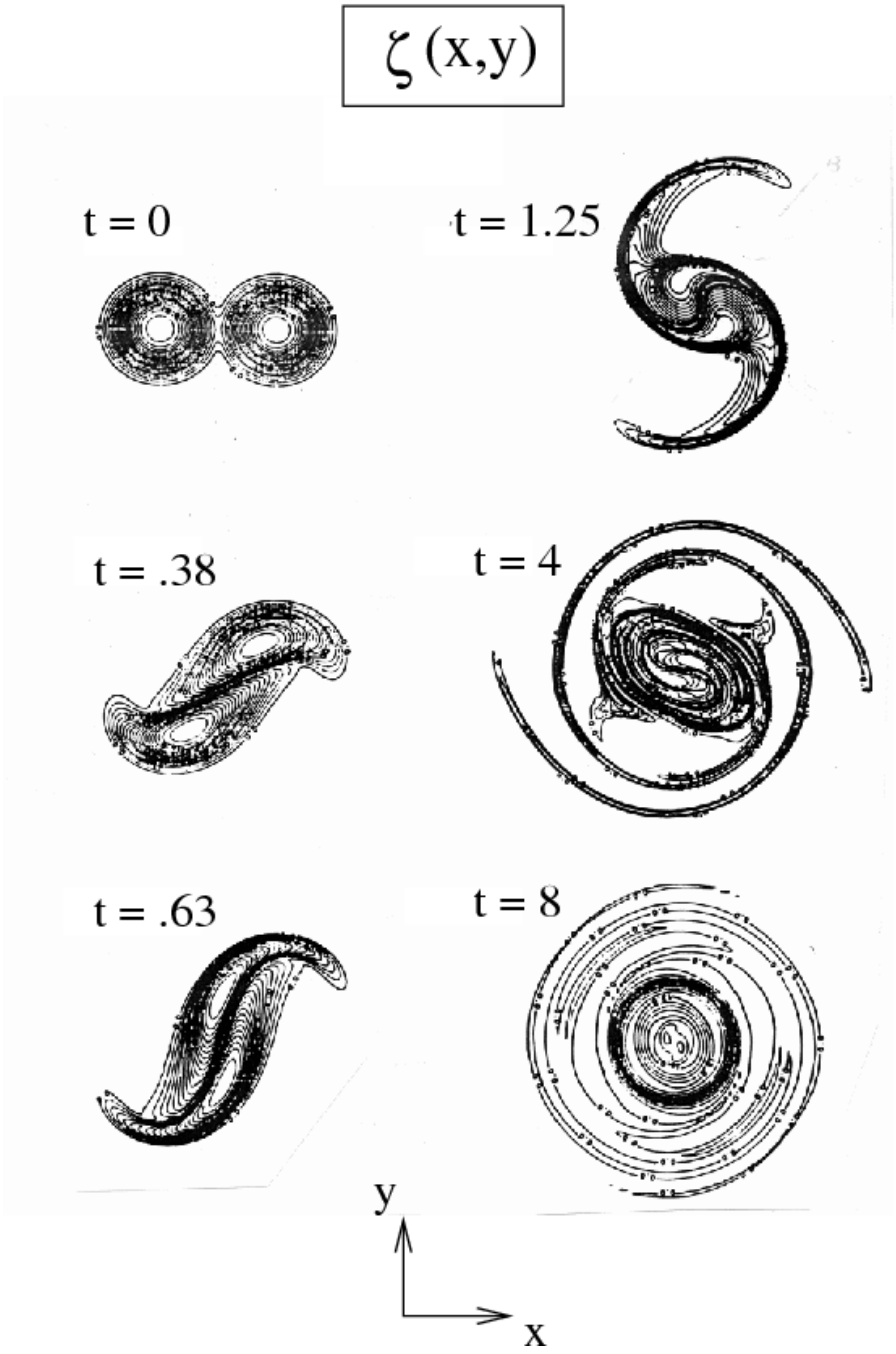

Figure 4: Computational solution for the merger of two like-sign, bare-monopole vortices (in non-dimensional time units scaled by L/V) initially located near each other. The exterior strain field from each vortex deforms the vorticity distribution of the other one so that the ζ fields wrap around each other; their centers move together along spiral trajectories; and ultimately they blend together after viscous diffusion smooths the strong gradients. While this is occurring, vorticity filaments are cast off from the merging vortices, stretched by the exterior strain field, and dissipated by viscosity. (Adapted from McWilliams, 1991.)

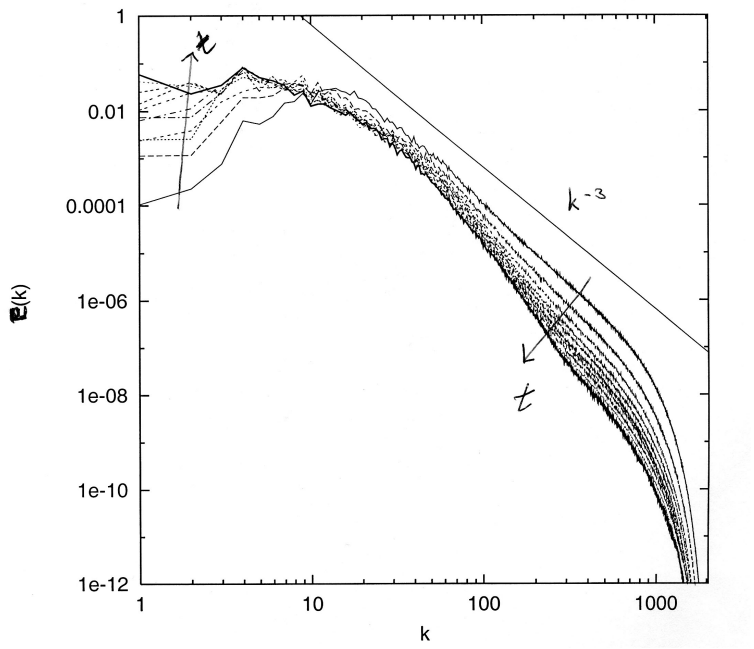

Figure 5: Evolution of the kinetic energy spectrum in decaying 2D turbulence at high Re. The different curves are for different times after initialization, with a general tendency toward lowering of $E(k)$ at high k and raising it at low k. (Bracco *et al.*, 2000)

ϵ does reach a small peak around $t = \tau_d$. With the dissipation of enstrophy at small scales, the enstrophy centroid $k_{ens}(t)$ reverses its direction and begins to follow the inverse cascade of the persistent (*i.e.,* non-cascading) component of the ζ field. Finally, in addition to all these trends associated with the second-moments of the solution, the kurtosis of the vorticity field $Ku(\zeta)$ (not shown), begins to grow for $t > \tau_d$, essentially without limit as long as the turbulent evolution continues. Here we define the average as a spatial one over the domain. A large value of Ku indicates significant spatial intermittency, and a growing value indicates increasing intermittency. This is a statistical indication of the emergence of, and subsequently increasing dominance of the ζ field by, the coherent vortices of 2D turbulence and of the the expanding area between the vortices where the vorticity field is weak. Another statistical measure of intermittency is the single-point PDF, shown in Fig. 6 for ζ at an intermediate time after the kurtosis has become large. The 2D PDF shows the $\sim$ exponential tails for large amplitude values that were discussed earlier as the nearly universal form for 3D turbulence at large Re (*cf.,* McWilliams, 2007); however, the 2D PDF form is quite different for small amplitude ζ values that become highly probable when the area between vortices is large.

3 Dynamical Control by Coherent Vortices

The dynamical control of 2D turbulence by coherent vortices can be demonstrated in several different ways. A direct way is by comparisons between solutions from a random initial condition (as in the preceding section) and other solutions that start from either vortex-absent or vortex-only ideal-

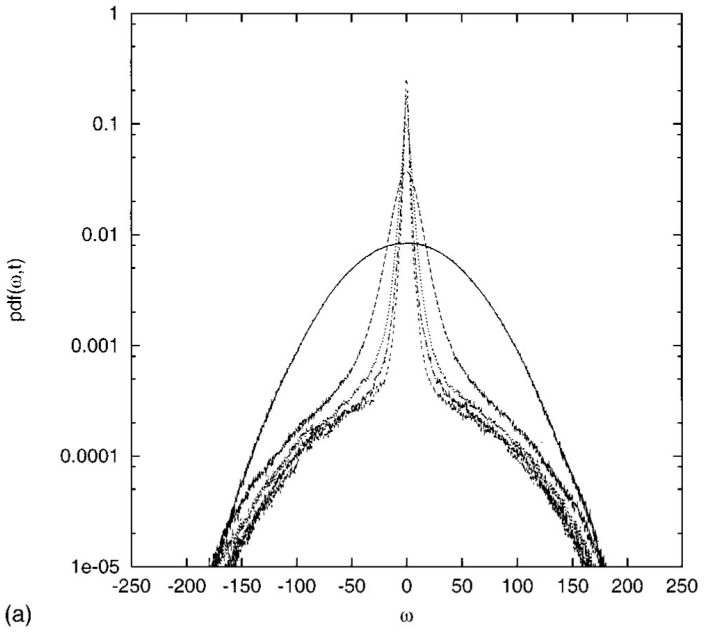

Figure 6: Evolution of the single-point PDF for vorticity in decaying 2D turbulence at high Re. The different curves are for different times after initialization (when the PDF is Gaussian), with a general tendency for increasing p for small $|\zeta|$, lowering of p for intermediate $|\zeta|$, and little change of p for large $|\zeta|$. (Bracco *et al.*, 2000)

izations of the original solution once it has evolved into a coherent state (McWilliams, 1990). The vortex-absent (v-a) state is obtained by preserving the amplitude (*i.e.,* the spectrum) but scrambling the phase of every Fourier component of the original solution at some time t_*,

$$\hat{\psi}_{v-a}(\mathbf{k}, t_*) \;=\; |\hat{\psi}_{orig}(\mathbf{k}, t_*)| e^{i2\pi r_{\mathbf{k}}}, \tag{12}$$

where $r_{\mathbf{k}}$ is a random variable uniformly distributed in $[0, 1]$. The subsequent vortex-absent evolution shows much more cascade and dissipation and much less intermittency until such time as coherent vortices re-emerge (Fig. 7). The vortex-only (v-o) idealized states are ones in which $\zeta(\mathbf{x}) \to \zeta_{v-o}(\mathbf{x})$ is set to zero at $t = t_*$ everywhere except in the vortex core regions, or additionally the core regions are made axisymmetric while preserving their circulation, or additionally their core positions are randomly scrambled. In all cases the subsequent statistical evolution is statistically similar to the original solution (*n.b.,* it cannot remain phase-coherent beyond a predictability time $\sim$ an eddy turnover time), except for an early paucity of small-scale variance in the spectrum that is filled soon in by the enstrophy cascade fed by vortex close encounters.

An indirect, but much more dynamically explicit, way of demonstrating vortex control is through the success of vortex-based dynamical systems (*i.e.,* vortex population-dynamics models; *cf., Turbulent Flows: General Properties*). The simplest one is a *mean-vortex theory* in which the N-vortex population distributions are assumed to collapse to a single value for size and strength, and the evolution occurs in a way that preserves both the core vorticity amplitude and the energy,

$$\zeta_o \;\sim\; t^0, \quad E \;=\; N\pi\zeta_o^2 R_o^4 \;\sim\; N\Gamma_o^2 \;\sim\; t^0\,, \tag{13}$$

where R_o is the vortex radius and $\Gamma_o = \pi\zeta_o R_o^2$ is the vortex circulation (Carnevale *et al.*, 1991).

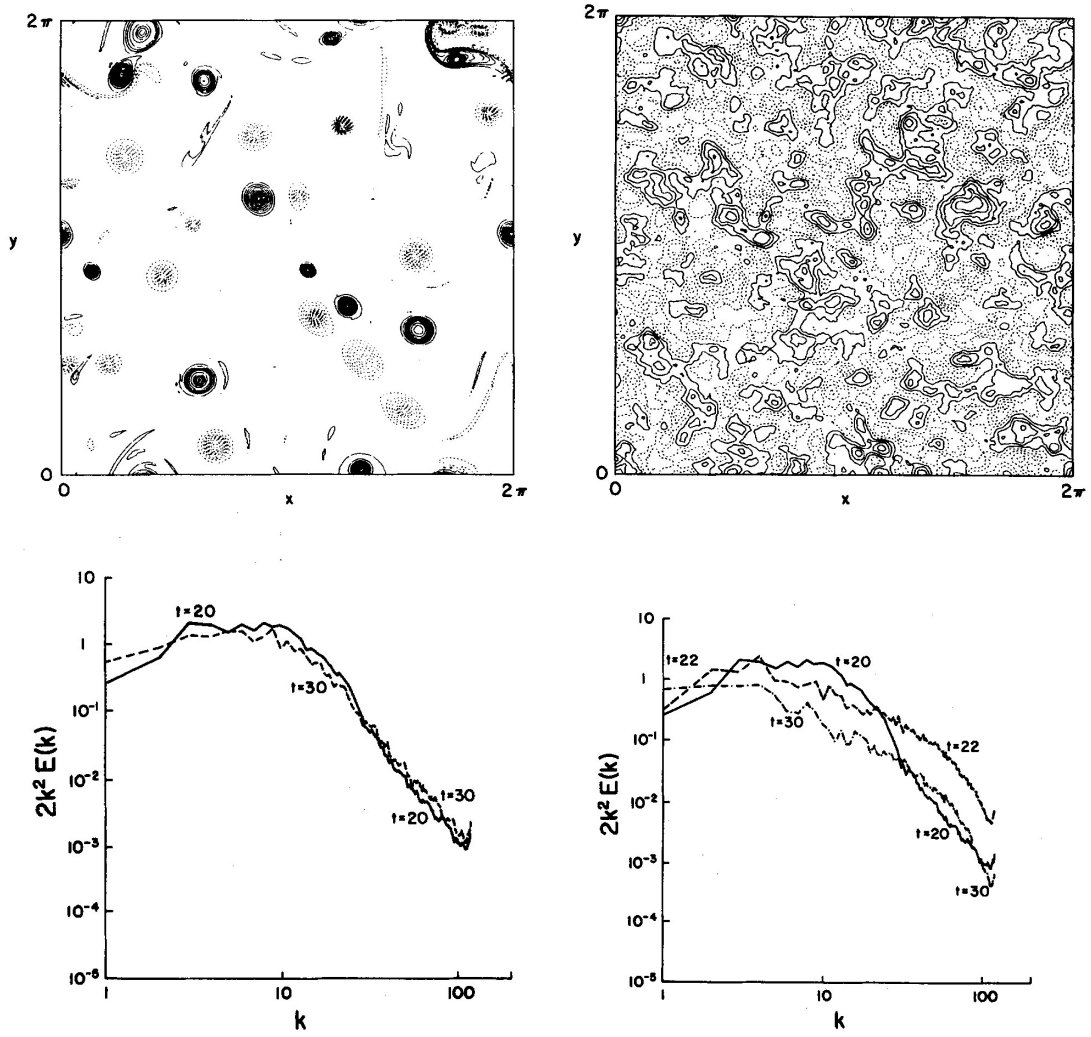

Figure 7: Vorticity snapshots $\zeta(x, y)$ at $t = 20$, (above) and enstrophy spectra (below) in 2D turbulence. The left column is for a decaying solution, and the right column is for a phase-scrambled field whose spectrum is equivalent to the decaying solution's at the scrambling time, and whose subsequent evolution shows much stronger cascade and dissipation until such time as new coherent vortices emerge (*e.g.,* after several time units). This shows how vortices control the turbulent evolution. (McWilliams, 1990)

With these constraints, plus an assumption that the population evolution can be self-similar in time, with the number of vortices decreasing as

$$N \sim t^{-\xi} \tag{14}$$

because of mergers (where $\xi \approx 0.72$ based on numerical solutions; (Fig. 8), the theory predicts

$$R_o \sim t^{\xi/4}, \quad \Gamma_o \sim t^{\xi/2} \tag{15}$$

for the vortex size and strength and with

$$\begin{aligned} Ens &= N\pi\zeta_o^2 R_o^2 \sim t^{-\xi/2} \\ Ku_\zeta &= \left(\frac{\text{Area}}{\pi}\right) \frac{N\zeta_o^4 R_o^2}{(N\zeta_o^2 R_o^2)^2} \sim t^{\xi/2} \end{aligned} \tag{16}$$

for these bulk statistical measures. These predicted behaviors are roughly confirmed in the numerical solutions for 2D turbulence, although the enstrophy decay there is faster than in the mean-vortex scaling theory, presumably because the latter implicitly assumes $Re \to \infty$.

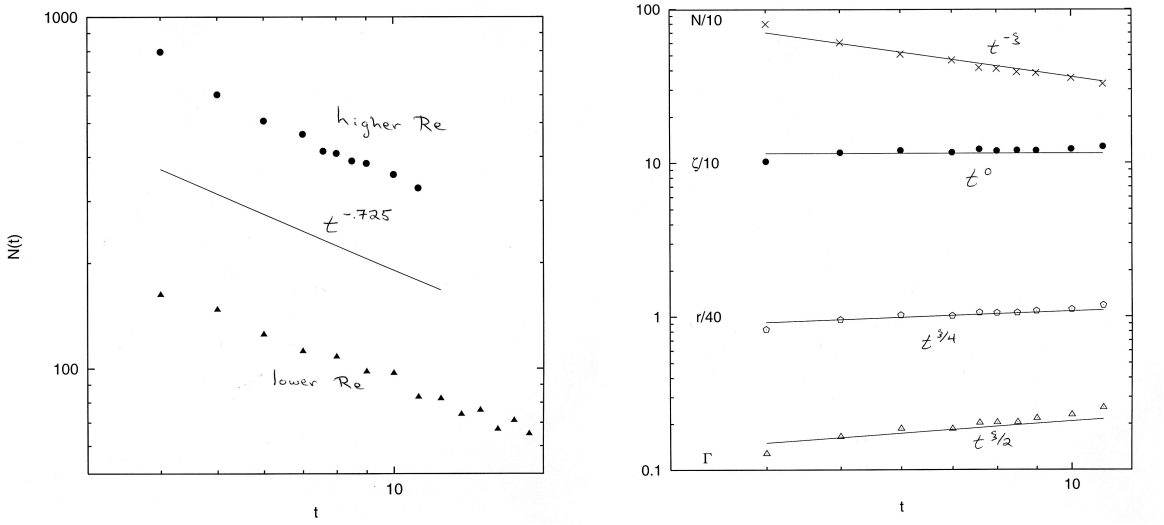

Figure 8: Evolution of vortex population statistics in decaying 2D turbulence: (Left) population number $N(t)$ in two solutions with higher (dots) and lower (triangles) values of Re. (Right) population N, average vorticity extremum ζ, average radial size r, and average circulation Γ in the solution with higher Re. (Bracco *et al.*, 2000)

A more general vortex-based dynamical system is one based on the conservative point-vortex model for vortex movement, but with evolutionary interruptions by abrupt, non-conservative events. The latter mimic mergers; their abruptness could be justified either by rapid completion of the merger (which is not strikingly true) or by the rapid dynamical decoupling of the local vortex pair interaction leading to merger and the movements of the vortex system as a whole, including the merging pair that has a bulk movement like a single vortex in addition to its local co-rotation. This, then, is an example of the approximate equivalence of loss of information from the large-scale degrees of freedom (*i.e.,* the coarse-grain representation by vortices) to smaller scales (the details of

the merging vortices and the associated vorticity filaments) and dissipation. To the point-vortex system, the abrupt merger transformation looks like a dissipative jump. This type of model is called *punctuated Hamiltonian dynamics* (pHd) (Weiss and McWilliams, 1993). The system is represented as N unequal vortices, with amplitudes $\zeta_i(t)$, radii $R_i(t)$, circulations Γ_i $(= \pi\zeta_i R_i^2)$, and positions $(x_i(t), y_i(t))$, $i = 1, ..., N$. The conservative part of the evolution is the Hamiltonian point vortex system, with

$$\begin{aligned} \dot{\zeta}_i &= \dot{R}_i = 0 \\ \dot{x}_i = \frac{\partial H}{\partial y_i}, &\qquad \dot{y}_i = -\frac{\partial H}{\partial x_i}\,, \end{aligned} \tag{17}$$

where $H(x_i, y_i, \Gamma_i)$ is the Hamiltonian for point vortices. The abrupt transformations occur when

$$|\mathbf{x}_k - \mathbf{x}_l| \leq D_{cr}(R_k, R_l) \text{ and } \frac{\zeta_k}{\zeta_l} > 0\,, \tag{18}$$

where D_c is the critical separation distance for the merger of unequal, like-sign vortices, as determined from the moment model. The consequent transformation rules for $(k, l) \to m$ have the same assumptions as in the mean-vortex theory, conservation of core vorticity and energy:

$$\begin{aligned} \zeta_m &= \zeta_l \times \max\left[1, \frac{\zeta_k}{\zeta_l}\right] \\ \Gamma_m^2 &= \Gamma_k^2 + \Gamma_l^2 \\ \mathbf{x}_m &= \frac{(\Gamma_k \mathbf{x}_k + \Gamma_l \mathbf{x}_l)}{(\Gamma_k + \Gamma_l)}\,. \end{aligned} \tag{19}$$

The pHd model asymptotically approaches the self-similar temporal scaling solution (13)-(16) with great precision, which itself seems to be a reasonably successful correspondence to the free evolution of 2D turbulence during its intermediate phase of a vortex-dominated evolution, following vortex emergence and preceding the approach to the dipole end-state. Its calculated temporal scaling exponent, $\xi \approx 0.7$, for population decay is essentially the same as in the fluid solutions However, the correspondence between the vortex population distribution functions of pHd and 2D turbulence is less precise (with relatively more small vortices in pHd) in the scaling regime, although it is still unclear how much this is due to excessive simplicity in the transformation rules (17)-(19) or to finite Re effects in the numerical solution for 2D turbulence. (Similar success has occurred using pHd to mimic fluid-dynamical solutions for equilibrium 2D turbulence with the addition of vortex generation and large-scale damping rules.) Recently Dritschel *et al.*(2008) revisited the population evolution problem and argued for a scaling exponent $\xi = 2/3$ based on an argument that vortex close encounters leading to merger are effected primarily by rapid dipole motions colliding with monopoles; phenomenologically, the evidence for this as a dominant vortex process is not entirely convincing, and in any event it is included among the behaviors occurring in the pHd model. LaCasce (2009) demonstrates that the population evolution exponent ξ can be associated with the dispersion rate (*i.e.,* $D \sim t^{1+\xi/2}$; also see Sec. 6 for a discussion of material transport)[4] for particles both inside and outside coherent vortices for the possibly lengthy interval

[4]The exponent $1 + \xi/2 \approx 1.35$ is indicative of "anomalous dispersion", *i.e.,* the exponent is not 1 and it is not expressive of an inertial cascade range. It implies that dispersion is not simply due to random passing of trajectories from one large eddy to a next one, and it also implies a degree of longer time correlation than in a random-walk conception.

in which mutual advection and merger of vortices is the dominant behavior (Sec. 2). This does not fully resolve the question of why ξ has the value it does, but it provides further support for the view that vortex motion dynamics determines vortex population and spectrum evolution.

4 Equilibrium Inertial Cascade Ranges

We can develop a 2D cascade theory, analogous to the Kolmogorov theory in 3D, by dimensional analysis and with the assumption that the cascade rate is independent of the spatial scale for $L_d < L < L_o$ (Kraichnan, 1967). There are two possible inertial cascade ranges for 2D turbulence. In an inverse *energy inertial cascade range*, we assume that ε is the scale-independent cascade rate toward larger scales, whence

$$E(k) \sim \varepsilon^{2/3} k^{-5/3} , \tag{20}$$

which has the same shape as in 3D (as it must have for dimensional consistency), albeit with a different interpretation of the role of ϵ. In a forward *enstrophy inertial cascade range*, we assume that $\hat{\eta}$ is the scale-independent cascade rate toward smaller scales (with dimensions of time^{-3}), whence

$$E(k) \sim \hat{\eta}^{2/3} k^{-3} , \tag{21}$$

which is a much steeper spectrum shape. The cascade of enstrophy to small scales implies a transition to the *enstrophy dissipation range* at a scale L_d defined by

$$L_d = \left(\frac{\nu^3}{\hat{\eta}} \right)^{1/6} , \tag{22}$$

which is analogous to the Kolmogorov dissipation length in 3D homogeneous turbulence.

These results allow us to posit an equilibrium spectrum $E(k)$ for 2D turbulence (Fig. 9). We assume that the system is somehow forced at a wavenumber, $k_f = 1/L_f$, much larger than the smallest available wavenumber in the domain and much smaller than the dissipation wavenumber, $k_d = 1/L_d$. The energy accumulation associated with the forcing moves towards larger scales with a spectrum shape (20). There is an implicit assumption that equilibrium is achieved because there is an energy sink on some very large scale since viscosity is ineffective at energy dissipation. Often boundary-layer (*i.e.,* Ekman) drag and radiative (*i.e.,* Rayleigh) damping are invoked as geophysically important large-scale energy sinks. The enstrophy accumulation associated with the forcing moves toward smaller scales with a spectrum shape (21). Enstrophy dissipation must occur in balance with the enstrophy generation by the forcing, and it can occur through viscous effects on $k \geq k_d$. In a loose geophysical interpretation of this spectrum, it is plausible to imagine that the high-k end of the anisotropic 2D cascade actually may be set by the transition to isotropic 3D turbulence; from this perspective the viscous dissipation in 2D turbulence is an eddy-viscosity surrogate for the missing 3D dynamics of nature. We will return below to a discussion of when and how well these equilibrium inertial ranges are realized in 2D turbulence.

The inertial-range spectrum shapes, justified most simply by dimensional reasoning, are the following:

- An inverse energy cascade range with a constant energy flux across wavenumbers ε [m^{2}s^{-3}] has the energy spectrum $E(k)$ [m^{3}s^{-2}] shape,

$$E(k) \propto \varepsilon^{2/3} k^{-5/3} .$$

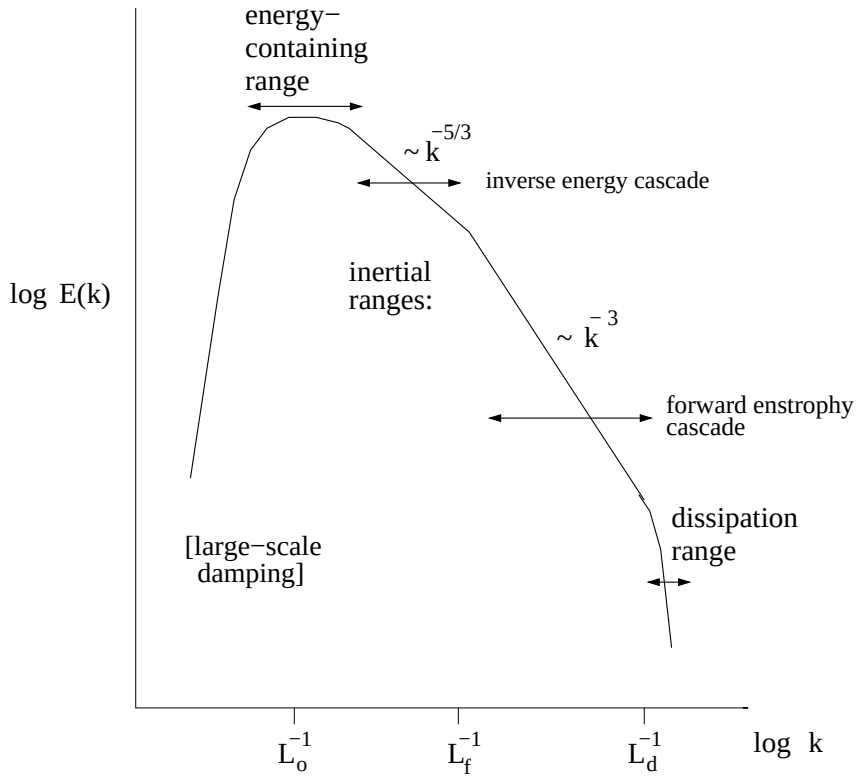

Figure 9: A cartoon of the isotropic kinetic energy spectrum in equilibrium 2D homogeneous turbulence, presuming a single source of forcing at an intermediate scale L_f.

- A forward enstrophy cascade range with a constant enstrophy flux across wavenumbers $\hat{\eta}$ [s^{-3}] has the energy spectrum shape,

$$E(k) \;\propto\; \hat{\eta}^{2/3} k^{-3}\,.$$

Notice that the former shape is identical to the 3D Kolmogorov shape, as it must be if it depends only on ε and k. However, the k-direction of the energy flux is opposite in 2D and 3D. Asymptotically in large scale separations among the domain, forcing, and dissipation lengths, the inverse enstrophy and forward energy fluxes, respectively, are vanishingly small in the energy and enstrophy inertial ranges.

We can make estimates for various quantities in the enstrophy range using an analogous phenomenological scaling theory. Given the k^{-3} spectrum shape, a velocity estimate at scale L is

$$V_L \;=\; \hat{\eta}^{1/3}\, L\,, \tag{23}$$

and the associated time scale is

$$\tau_L \;=\; \hat{\eta}^{-\,1/3}\,. \tag{24}$$

The dissipation scales are

$$L_d \;=\; \left(\frac{\nu^3}{\hat{\eta}}\right)^{1/6} \;=\; L_0 \left[\frac{\hat{\eta}}{(V_0/L_0)^3}\right]^{-\,1/6} Re^{-\,1/2} \quad \text{and} \quad \tau_d \;=\hat{\eta}^{-\,1/3} \;=\; \frac{L_0}{V_0}\left[\frac{\hat{\eta}}{(V_0/L_0)^3}\right]^{-\,1/3}\,; \tag{25}$$

hence, the size of a turbulent event is

$$\left(\frac{L_o}{L_d}\right)^2 \times \frac{\tau_o}{\tau_d} \;=\; \left[\frac{\hat{\eta}}{(V_0/L_0)^3}\right]^{2/3} Re\,. \tag{26}$$

Thus, compared to their 3D counterparts, the enstrophy inertial-range velocity is much weaker, the time scale is much longer (and independent of Re), and the size of a turbulent cascade event is much smaller. In particular, the ratio of 2D and 3D event sizes is $\propto Re^{-\,7/4}$, implying enormous measurement and computational advantages in 2D. (This estimate does not take into account the potentially very long lifetime of the coherent vortices in 2D (Fig. 10), lasting for many cascade events.)

Computational simulations have also been made of *equilibrium 2D turbulence* (*cf.,* decaying turbulence in Sec. 2). To achieve equilibration in the presence of viscosity, a sustained excitation source is needed and, because of inverse cascade, an extra energy sink is needed at large scales since ν is ineffective at energy dissipation. An extension of (3) with these features is

$$\frac{D\zeta}{Dt} \;=\; F + \mu\psi + \nu\nabla^2\zeta\,. \tag{27}$$

F [s^{-2}] is a random forcing; the scales where it acts can either be relatively large if the focus is on the forward enstrophy cascade or small if the focus is the inverse cascade. μ [$m^{-2}s^{-1}$] is a "hypo-viscous" damping coefficient. Both F and μ are artifices compared to more realistic forcing in nature from unstable mean currents and large-scale dissipation from infrared radiation or bottom drag. As long as $|F|$ is small compared to the enstrophy and Re is large, coherent vortices (Fig.

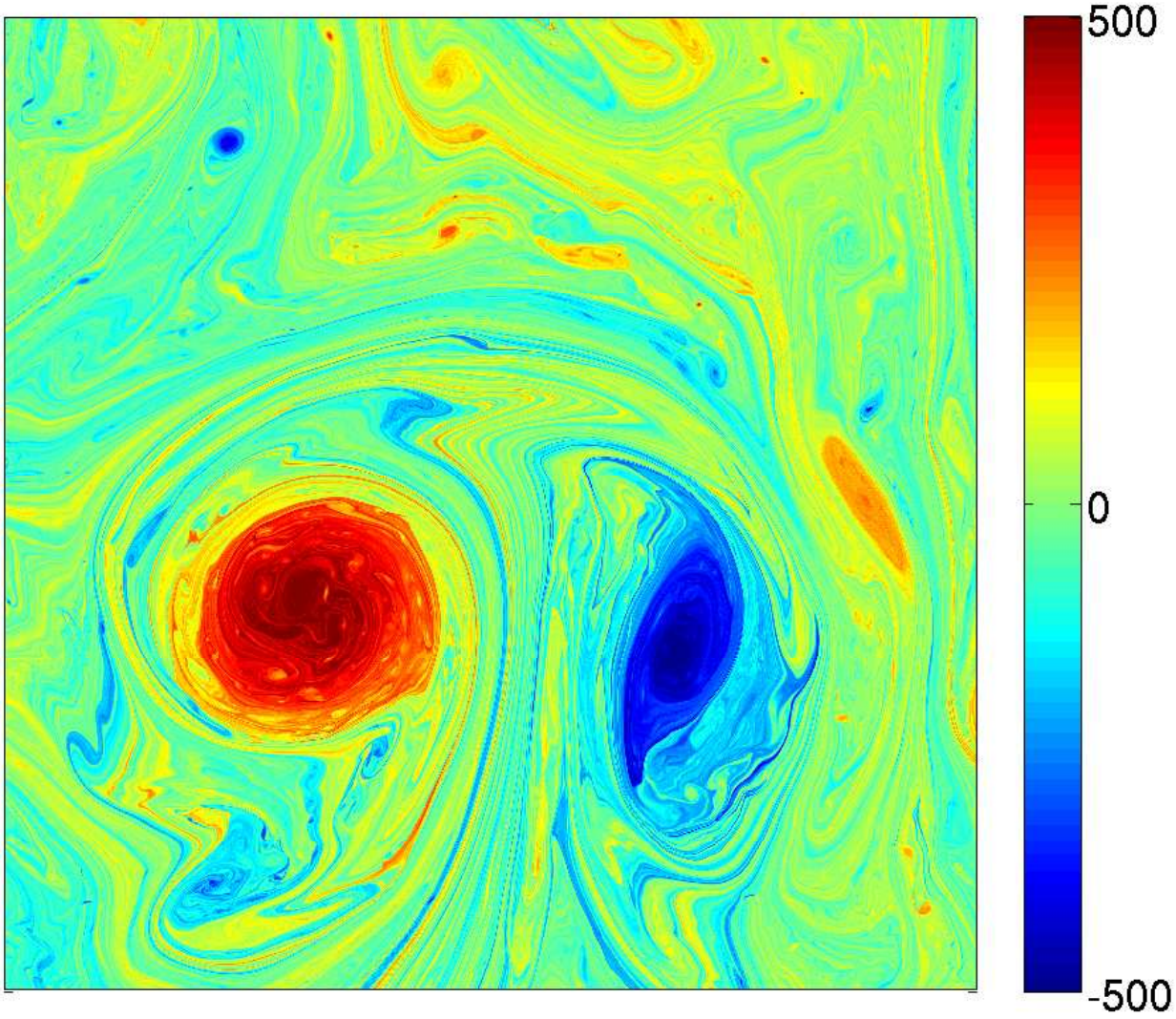

Figure 10: Instantaneous vorticity field $\zeta(x, y)$ in equilibrium 2D turbulence in one-quarter of a doubly periodic domain at high Re. Notice the multiply-folded filaments between the coherent vortices near the forcing scale, the internal fluctuations within the dominant dipole, and the much finer-scale vortices in the far-field regions with weak large-scale strain. This solution has a spectrum close to $E \propto k^{-3}$ on scales smaller than F. (Bracco and McWilliams, 2010)

10) and strong intermittency can coexist with the expected inertial cascades. Notice that there is interesting interior structure in the large-scale vortices when Re is large enough.

Figure 11 shows the spectrum (with $k = 1$ the largest wavenumber in a domain of size 2π) and the PDF for ζ in equilibrium 2D turbulence (27). These are from a sequence of solutions with increasing grid size $N \times N$ and decreasing ν (hence increasing Re), with the large-scale random forcing F and damping coefficient μ unchanging. The spectrum both increases in overall energy level and convincingly approaches a k^{-3} shape as Re increases, thereby confirming the expectation of an enstrophy inertial-cascade range. This range also extends to higher wavenumbers as the enstrophy dissipation scale L_d in (22) decreases with smaller ν. The PDF is plotted against vorticity magnitude (combining both signs since this variable is parity symmetric here) and normalized by the standard deviation of ζ, which does increase with Re. The PDF is approximately invariant with Re, apart from some non-systematic variability in the tail reflecting a finite averaging time. In particular, a characteristic intermittency measure, $Ku[\zeta] \approx 7.2$, and it scales approximately as Ro^0, quite different from its scaling as $Re^{1/3}$ in equilibrium 3D turbulence. This is because intermittency in 2D is controlled by the large- and medium-sized coherent vortices that do not strongly change with Re, whereas in 3D the intermittency is dominated by flow structure near the Kolmogorov scale, $L_d \sim Re^{-3/4}$ (***3D Homogeneous Turbulence***).

Another result from Bracco and McWilliams (2010) is that different random forcing statistics, in particular the forcing correlation time, lead to different Re scaling exponents for the bulk properties of the flow (***e.g.,*** energy, enstrophy, η) and a different values for the asymptotic intermittency measure $Ku[\zeta]$, even though the energy spectrum shape continues to approach the inertial range form, k^{-3}. This implies that 2D turbulence is a non-universal regime, and the reason for this is that different problems will have different populations of coherent vortices at larger scales where the random forcing acts.

The inertial ranges of 2D turbulence have provided a simple standard against which to compare atmospheric and oceanic spectra (Fig. 12). Motions on the synoptic scale in the extra-tropical atmosphere have an approximately k^{-3} velocity and temperature spectrum shape, and oceanic mesoscale motions in the ocean have an approximately k^{-5} shape for sea level (as would be expected for pressure in geostrophic balance with velocity; ***i.e.,*** $\hat{\phi} \sim \hat{u}/fk$). Furthermore, the atmospheric mesoscale spectrum shows an approximately $k^{-5/3}$ shape for velocity in a scale range where the velocity field is highly anisotropic (with $w \ll u, v$) so the flow is not like 3D homogeneous turbulence. Of course, none of these regimes are two-dimensional. So, the rationalization of relevance is that geostrophic and stratified turbulence regimes can share these inertial range shapes with 2D turbulence. For the enstrophy inertial range, the assumed "forcing" is the instability of mean currents (***e.g.,*** jet stream and Gulf stream) at scales just larger than the inertial range. For the atmospheric mesoscale, the assumed forcing is at the convective scale $\sim 1 - 10$ km. Lilly (1989) argued that equilibrium 2D turbulence with both large- and small-scale forcing would have a large-scale enstrophy range and small-scale energy range, with their respective cascade fluxes passing through each other without disruptive interference (Fig. 13). We have to impose these as forcings somewhat arbitrarily in our 2D dynamics since their true fluid dynamics involves 3D motions. Although it is undoubtedly too simplistic to expect 2D turbulence to be an adequate model for geophysical turbulence, it nevertheless is suggestive that it seems consistent with the gross distributions of synoptic and mesoscale energy in nature.[5]

[5]In the case of the atmospheric mesoscale spectrum, Callies *et al.* (2015) have recently demonstrated that it is more

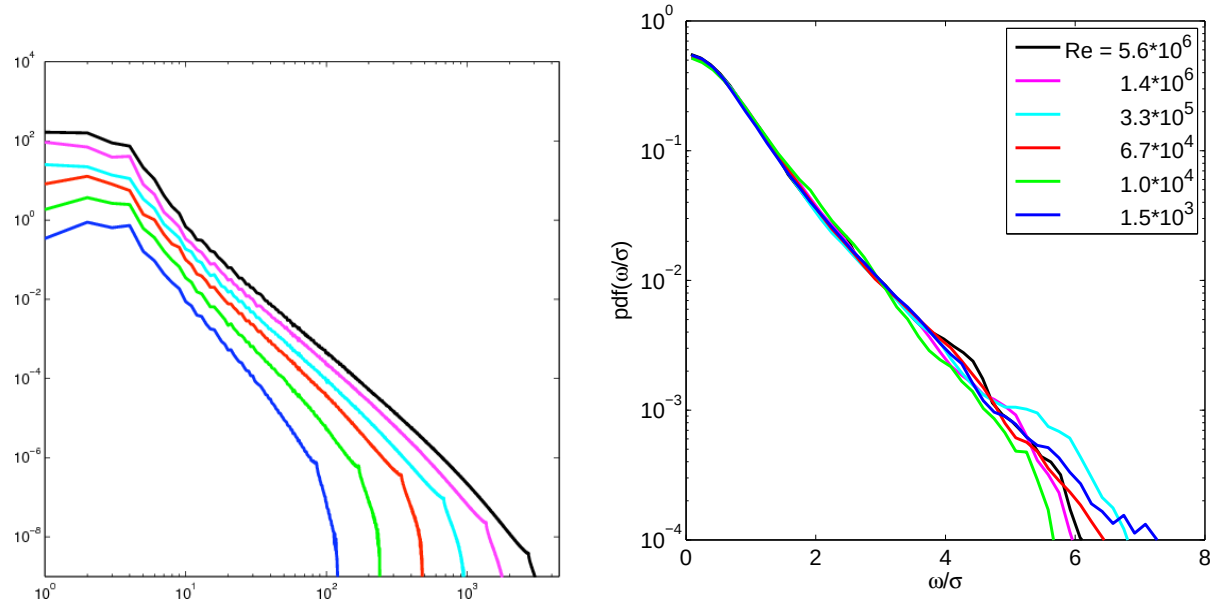

Figure 11: Statistical measures of equilibrium 2D turbulence at a sequence of horizontal grid sizes $N \times N$ and Re values, ranging from ($N = 256,\ Re = 1.5 \times 10^3$) to ($N = 8096,\ Re = 6 \times 10^6$): (left) kinetic energy spectrum $E(k)$; (right) PDF of vorticity, $\omega = |\zeta|$, normalized by its standard deviation σ. The curves are labeled by Re. (Bracco and McWilliams, 2010)

Probably a modern consensus is something very like a forward enstrophy cascade is realized in the atmosphere and ocean on the larger mesoscales, but the possibility of an inverse (kinetic) energy cascade on the smaller mesoscales is restricted to the "surfaces" (*cf., surface quasigeostrophy*; Capet *et al.*, 2008a) rather than the volumetric interiors where the energy cascades, if any, are more likely to be in the forward direction. (But non-geostrophic models of the surface layer in the sub-mesoscale range do exhibit forward kinetic energy cascades; Capet *et al.*, 2008b).

We can estimate the magnitudes of various quantities in the inertial ranges, as in the 3D case. For the energy range, the estimates are the same as in 3D, given the different interpretation of ϵ. For the enstrophy range, the estimates are

$$V_L \ = \ \hat{\eta}^{1/3} L, \quad \zeta_L \ = \ \hat{\eta}^{1/3}, \quad \tau_L \ = \ \hat{\eta}^{-1/3} \ . \tag{28}$$

Note that both the vorticity amplitude and the advective time scale are independent of the length. The former means that a Taylor microscale is ill-defined in this range since the vorticity spectrum will not have a sharply defined peak (*i.e.,* $k^2 e \sim k^{-1}$ here) until a small enough scale is reached so that viscosity depletes the spectrum amplitude (*n.b.,* viscosity is also necessary in 3D turbulence for the Taylor microscale to be well defined). From the earlier estimate of $\hat{\eta} \ = \ Ens^{3/2}$, we can replace the time scale here with $\hat{\eta}^{-1/3} \ = \ Ens^{-1/2}$.

consistent with internal-wave dynamics than with geostrophic dynamics that might be analogous to 2D turbulence. This interpretation is also consistent with the modern understanding of stably stratified turbulence that its energy cascade at large Re is in the forward direction.

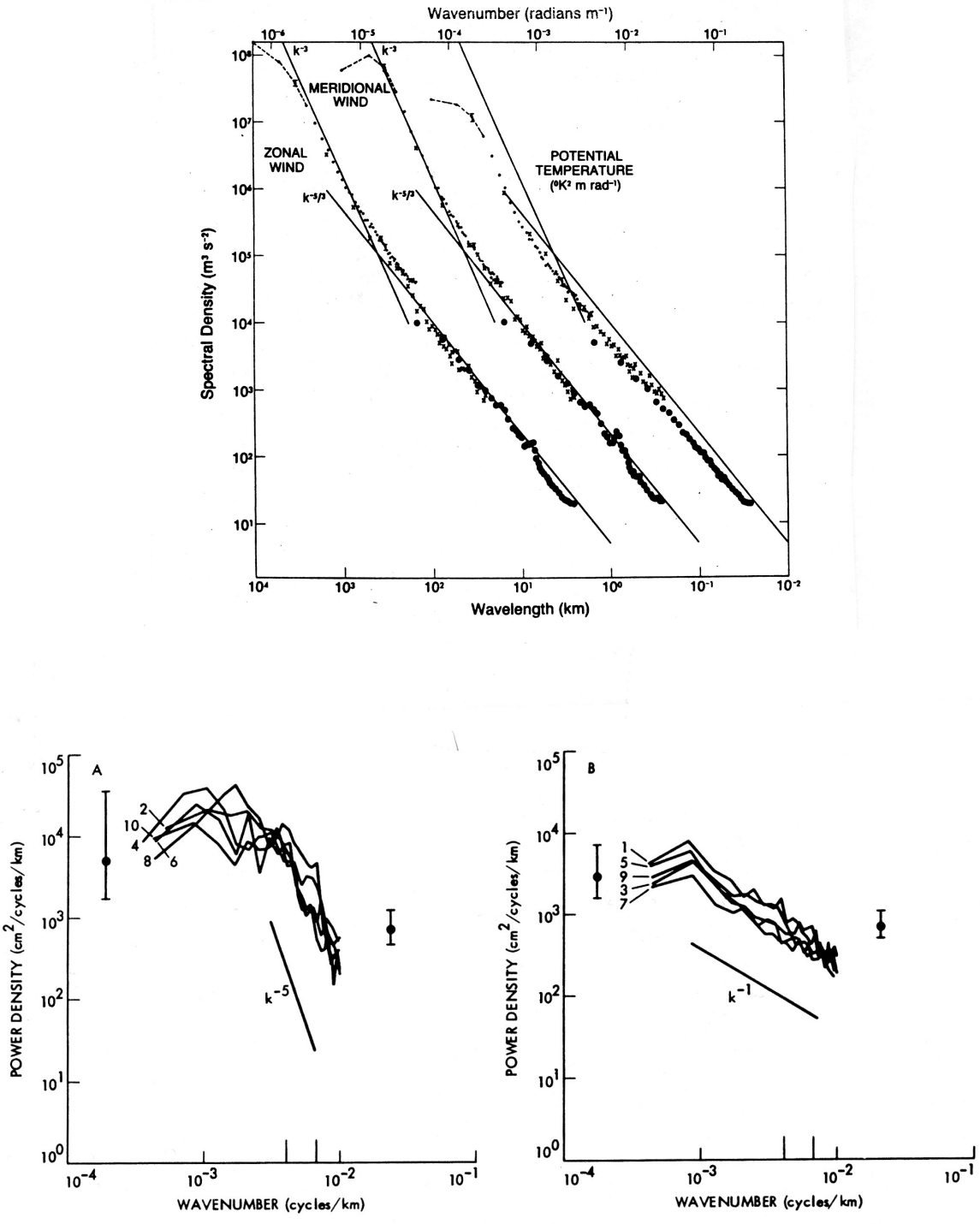

Figure 12: Measured spectra of kinetic energy near the tropopause in the atmosphere (left; Nastrom and Gage, 1985) and and sea-surface dynamic height in the ocean (right; Fu, 1983). The reference power laws, based on 2D turbulence inertial ranges, for the former are k^{-3} and $k^{-5/3}$, consistent with a forward enstrophy cascade from large-scale forcing and an inverse energy cascade from small-scale forcing. The reference power law for the latter is k^{-5}, consistent with a k^{-3} velocity spectrum, geostrophic balance between horizontal velocity and surface dynamic height (pressure), and a forward enstrophy cascade from large-scale forcing.

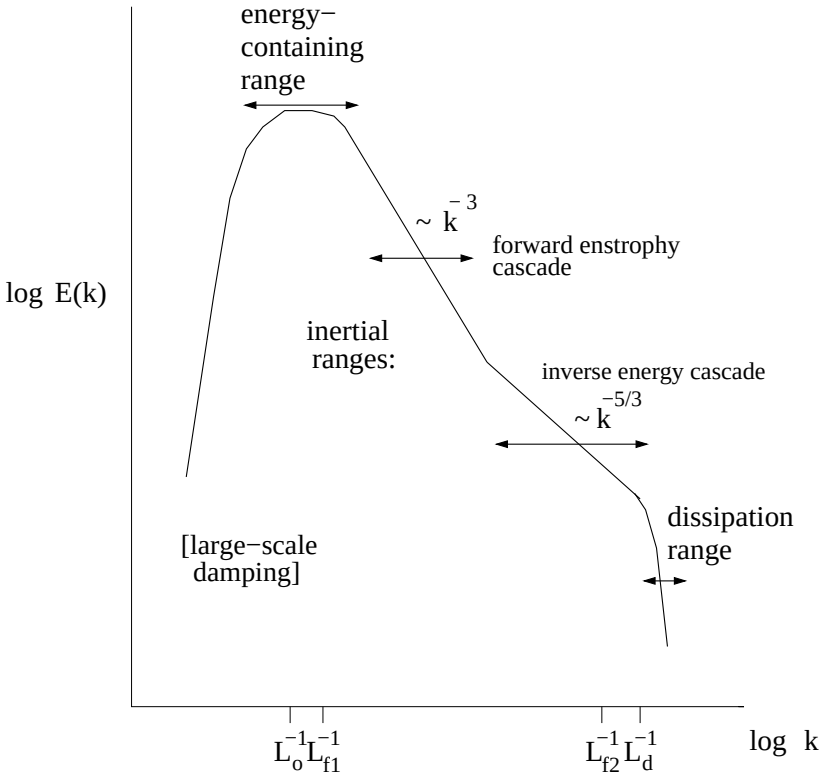

Figure 13: A cartoon of the isotropic kinetic energy spectrum in equilibrium 2D homogeneous turbulence, presuming two sources of forcing at large and small scales, L_{f1} and L_{f2} respectively (*cf.,* Lilly, 1989).

5 Predictability in 2D

Using these estimates, we can estimate the predictability horizon within the enstrophy cascade range, analogous to the 3D energy-range estimates that also apply to the 2D energy range. Again, the phenomenological model for the evolution of the bounding wavenumber $k_p(t)$ between predictable and unpredictable portions of the spectrum is the following:

$$\frac{dk_p}{dt} \;=\; -\frac{k_p}{\tau_k}, \quad k_p(0) \;=\; k_* \tag{29}$$

where now $1/\tau_k \;=\; Ens^{1/2}$, a constant with respect to k_p. Thus, the solution is

$$k_p(t) \;=\; k_* \exp\left[-Ens^{1/2}t\right]. \tag{30}$$

Note that k_* never becomes negligible in this formula, unlike 3D. Furthermore, the predictability horizon time T_p–defined as the time it takes k_p to reach the large-scale end of the enstrophy range k_o–is

$$T_p \;=\; Ens^{-1/2} \log\left[\frac{k_*}{k_o}\right] \;=\; Ens^{-1/2} \log[Re_*]\,, \tag{31}$$

where Re_* is a Reynolds number based on the initial ignorance scale L_*. Thus, as $Re_* \to \infty$, $T_p \to \infty$ (unlike in 3D), although the rate of increase is with a slow logarithmic dependence so that in practice T_p will be only a modest multiple of the advective turn-over time $Ens^{-1/2}$. Note that the logarithmic dependence on Re here is like that of the dissipation onset time. From these dependencies, in contrast with the independence of Re in the 3D energy cascade, we can say that the 2D enstrophy cascade is a less efficient.

6 Material Transport

As a final topic we consider material transport in 2D homogeneous turbulence as measured by the statistical behavior of individual parcel trajectories. On a sufficiently long time scale $\tau \gg \tau_\zeta$, the dispersion $D(\tau)$ does seem to approach a linear function of τ, indicating a random-walking behavior. However, this time can be very long, because parcels can both be trapped within vortex cores or excluded from them for very long time intervals (Fig. 14). There seems to be no process that will bring a parcel into the core of a surviving vortex, and parcels on the periphery of a vortex will circulate around and be carried with it until some close vortex interaction strips it away. Thus, the time for a passive tracer field to become well mixed everywhere is very long in 2D turbulence, although the vortex exterior region (*i.e.,* the majority of the area in the domain) becomes well mixed after a time of only $\mathcal{O}(\tau_\zeta)$.

We compare a Lagrangian stochastic diffusion model of particle dispersion (Sec. 4 of *3D Homogeneous Turbulence* notes) with the results of a 2D turbulence simulation after a time interval on several eddy recirculation times (Fig. 15). It is clear that there is relatively more clumping of particles with small pairwise separation distances in 2D than is consistent with diffusion. Particle trapping in and near the coherent vortices is the primary reason.

A phenomenological theory for dispersion can be developed for the 2D enstrophy inertial range, analogous to the one in Sec. 4 of *3D Homogeneous Turbulence* notes. We start with the Lagrangian

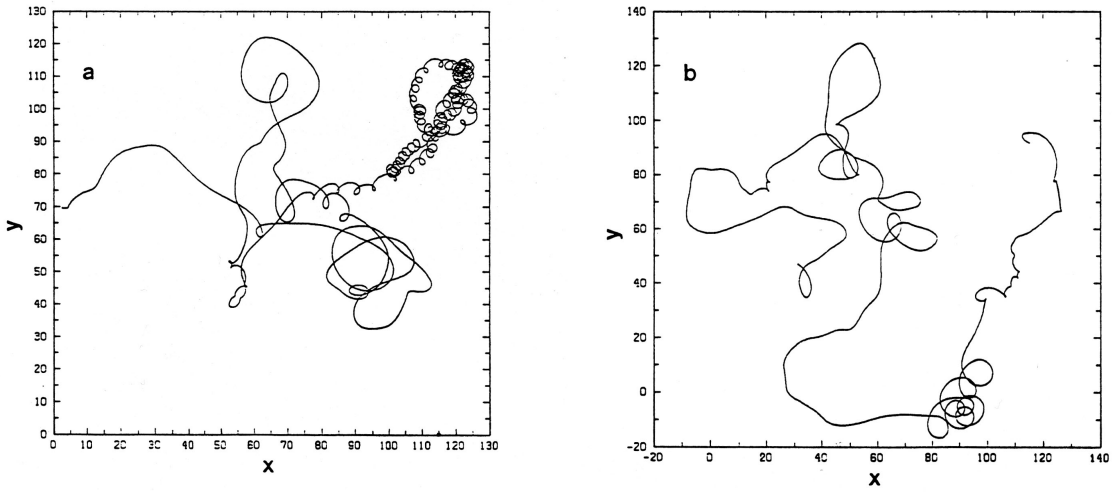

Figure 14: Trajectories of two advected parcels initially seeded into different regions in equilibrium 2D turbulence. The axis scales are in units of the computational grid spacing. The left panel shows a parcel seeded inside a vortex, while the right panel shows a parcel seeded in the region outside the vortices. Parcels do not enter the cores of vortices, and parcels within vortices stay inside for as long as the vortex survives. (Provenzale *et al.*, 1995)

diffusivity definition and estimate its right-hand side with an inertial range correlation time scale, $t_c \sim \eta^{-1/3}$:

$$\kappa = \frac{d}{dt} D \sim \frac{D}{t_c} \,. \tag{32}$$

Since this t_c is independent of time since release and/or parcel separation distance, the result is exponential dispersion,

$$D(t) \sim \exp[\eta^{1/3} t] \,, \tag{33}$$

with a corresponding κ that is also exponential. (For the 3D energy inertial range, we choose $t_c \sim \varepsilon^{-1/3} D^{1/3}$, equating D with the local scale L^2. The result is $D(t) \sim \varepsilon t^3$; *i.e.,* Richardson's law in eq. (33) of the 3D notes.) An observational evaluation for D on separation scales of 100s km in the atmospheric stratosphere in Fig. 16 is consistent with exponential dispersion among balloon pairs in (33). LaCasce (2010) shows other consistent evidence from the ocean over mesoscale separation distances. Both indicate that 2D turbulence is relevant to mesoscale and synoptic scale flows in nature.

A simple depiction of exponential separation behavior comes particle trajectories in a a uniform strain flow in 2D; *e.g.,*

$$u = -\alpha x \,, \qquad v = \alpha y \,, \tag{34}$$

where α is a strain rate assumed constant. This flow is steady and it has neither divergence nor vorticity. It can be viewed as an idealization of the far-field flow in the neighborhood of a coherent vortex. We solve trajectory equations for $\mathbf{X}(t)$ in this flow:

$$\frac{dX}{dt} = -\alpha X \,, \qquad \frac{dY}{dt} = \alpha Y \,. \tag{35}$$

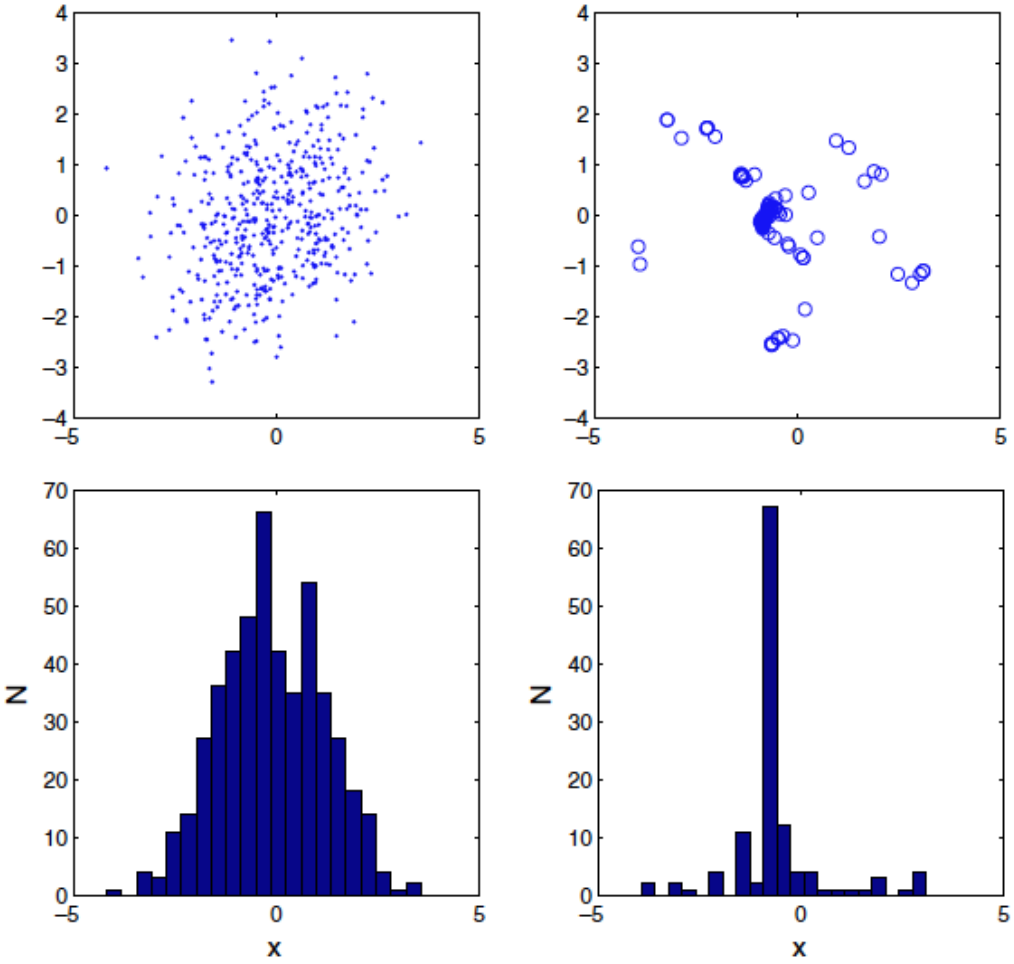

Figure 15: Two examples of particle advection. The 484 particles in the upper left panel have been advected by the stochastic model (eq. (30) of *3D Homogeneous Turbulence* notes), while the 121 particles in the upper right panel were advected by a 2D turbulent flow. The lower panels show histograms of the x-displacements. (LaCasce, 2008)

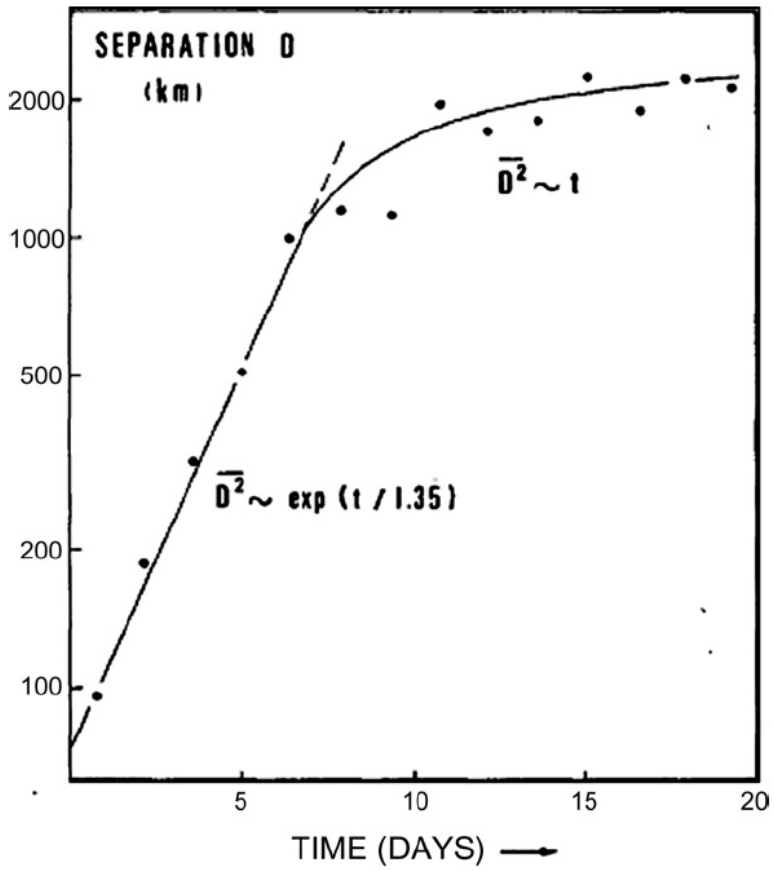

Figure 16: Dispersion vs. time for the EOLE balloon pairs in the stratosphere. The symbol $\overline{D^2}$ here is the same as D in Sec. 4 of *3D Homogeneous Turbulence* notes. Notice the exponential dispersion for smaller times, consistent with the enstrophy inertial range of 2D turbulence. At late times the dispersion is approximately linear, consistent with diffusion by large eddies. (Morel and Larcheveque, 1974)

The solutions are exponentials,

$$X(t) = X(0)e^{-\alpha t}\,, \qquad Y(t) = Y(0)e^{+\alpha t}\,, \tag{36}$$

and in particular the distance between two parcels with different initial locations in y will grow exponentially in time. In 2D turbulence the vortices on scales larger than the enstrophy inertial range provide a slowly varying strain field that causes the dispersion behavior in (33)[6].

7 2D Turbulence in a Bounded Domain

Now assume that there are no-normal flow and no-slip boundary conditions of the side of a finite-size 2D domain. This, of course, violates the homogeneity assumption, but nevertheless it provides an early view of boundary-layer shear turbulence, and it might be viewed as a relevant analog model for oceanic geostrophic turbulence which does have a bottom that rises to the surface at the coastline, hence has a no-slip side boundary condition of sorts. (Actually the physically relevant boundary stress is at the bottom, but still it has the effect of making the horizontal flow approach zero at the coastline.) Because this problem has only two spatial dimensions, it is much more computationally accessible than the 3D problems just mentioned.

The most important new behavior in a bounded domain is that any flow near the boundary, *e.g.,* due to a coherent vortex, will induce a boundary layer with vorticity of the opposite sign and with a magnitude that is larger as the boundary layer gets thinner, as happens when the Re value gets larger (Fig. 17). This means that even in a freely decaying problem, there is an enstrophy source near the boundary, although the energy decay continues to be monotonic.

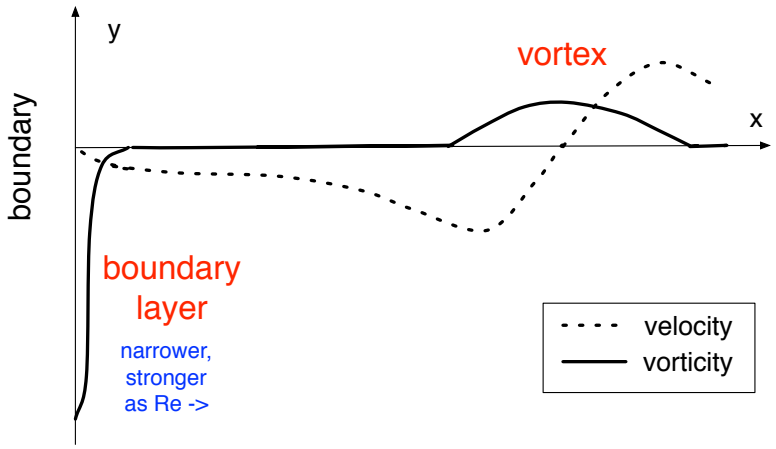

Figure 17: Sketch of the velocity and vorticity for a coherent vortex near a no-slip boundary. A boundary layer develops adjacent to the boundary, and its associated vorticity is of the opposite sign with a magnitude that increases without bound as $Re- > \infty$.

There is a modest literature on this problem, focusing on free decay (*e.g.,* Clercx *et al.*, 2009). Recently with a colleague, Guillaume Roullet, we have revisited this problem for both free decay

[6]Notice the similarity of the larger-scale flow structures and the smaller-scale effects in the different contexts of vortex stretching in 3D (Sec. 7 of the 3D notes) and material dispersal in 2D.

and randomly forced equilibrium cases in a variety of domain shapes. The novelty of our approach is a subgrid-scale parameterization for both the interior dissipation and the boundary-layer vorticity generation that allows us to achieve much higher Re than previously and one with a time-amplitude symmetry that is consistent with never reaching a late-time viscous decay phase as the flow amplitude decreases (*i.e.,* the advective time-scale evolution merely slows down as the energy decays). The work is not yet published.

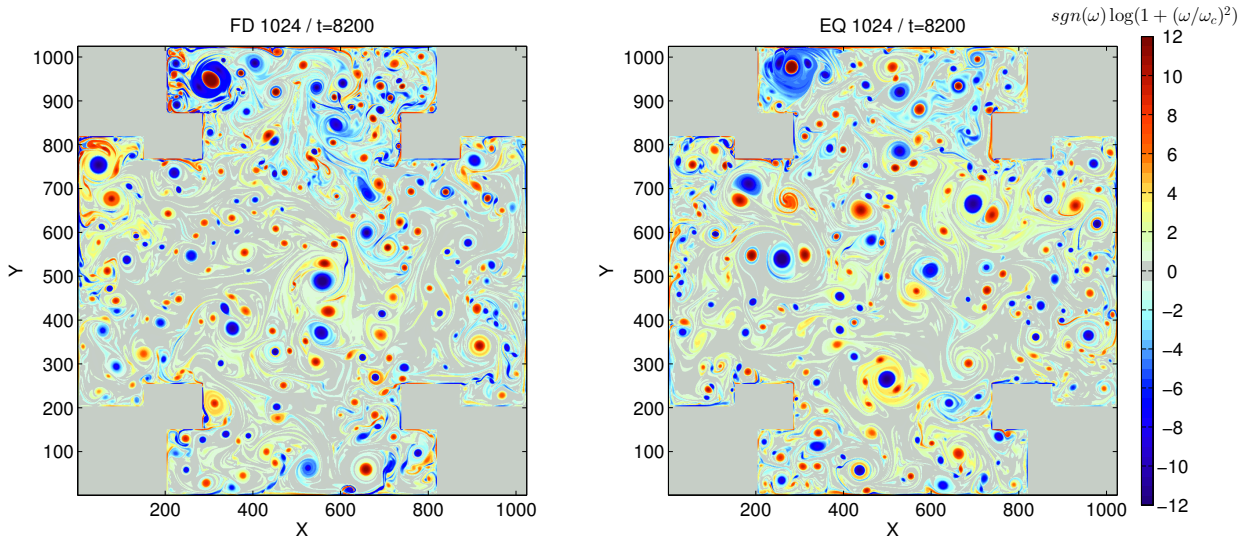

Figure 18: Snapshots of the vorticity (here $\zeta = \omega$) with a sign-preserving logarithmic scale to see a large amplitude range. The left figure is from a free decay problem (FD) in an irregular domain (note the black land mask) with large Re, and the right one is from a randomly forced statistical equilibrium problem (EQ) with the same Re. The grid resolution is $N = 1024$ in each direction. Both plots are at late times when the flow is either self-similarly evolving with a slow decay of energy (FD), or fluctuating about stationary statistics for energy, enstrophy, *etc.* Notice the abundance of coherent vortices of both signs, the thin strips of vorticity in the boundary layer, and flow separation from the boundary followed by vortex-filament instability and vortex roll-up to form new coherent small-scale vortices. Some interior vortices have undergone mergers to grow in size, but no vortex survives indefinitely long because of occasional destructive close-encounter interactions with the boundaries.

An illustration of the flow fields for free-decay (FD) and forced-equilibrium (EQ) states is in Fig. 18. As we have come to expect in 2D turbulence, the flow is dominated by coherent vortices. Without going into much detail about these results, I'll simply remark that the existence of the boundaries alters the system evolution in several important ways:

- The self-similar distribution of vortex shapes in the late-time FD evolution involves a continual vorticity generation at small scales near the boundary, upscale energy cascade in the interior, and intermittent large-vortex destruction during close approaches to the boundary. This is inconsistent with inertial-range cascades as are found in unbounded and periodic-domain 2D turbulence.

- In particular, for large enough Re in FD, there is no approach at late-time to a few-vortex

non-turbulent end-state as occurs in a finite-size periodic domain. Instead, the continual regeneration of small vortices near the boundary maintains a stable, many-vortex population distribution.

- In EQ for large enough Re, there is no need for an "artificial" large-scale energy dissipation mechanism, unlike in a periodic domain. The vortex destruction process for large-vortices that come close enough to the boundary is sufficient to arrest the inverse energy cascade before it reaches the domain scale.

Thus, 2D turbulence in a bounded domain provides a better analog dynamics for real geophysical flows insofar as it does not exhibit the "unnatural" behaviors of a non-turbulent FD end-state or the necessity of a large-scale dissipation process in EQ.

References

Batchelor, G.K., 1953: *The Theory of Homogeneous Turbulence*. Cambridge.

Bracco, A., J.C. McWilliams, G. Murante, A. Provenzale, and J.B. Weiss, 2000: Revisiting two-dimensional turbulence at millennial resolution. *Phys. Fluids* **12**, 2931-2941.

Bracco, A., and J.C. McWilliams, 2010: Reynolds-number dependency in homogeneous, stationary two-dimensional turbulence. *J. Fluid Mech.* **646**, 517-526.

Callies, J., R. Ferrari, and O. Bhler, 2014: Transition from geostrophic turbulence to inertia-gravity waves in the atmospheric energy spectrum. *Proc. Nat. Acad. Sciences* **111**, 17033-17038.

Capet, X., P. Klein, B.L. Hua, G. Lapeyre, and J.C. McWilliams, 2008a: Surface kinetic energy transfer in SQG flows. *J. Fluid Mech.* **604**, 165-175.

Capet, X., J.C. McWilliams, M.J. Molemaker, & A. Shchepetkin, 2008b: Mesoscale to submesoscale transition in the California Current System. III: Energy balance and flux. *J. Phys. Ocean.* **38**, 2256-2269.

Carnevale, G.F., J.C. McWilliams, Y. Pomeau, J.B. Weiss, and W.R. Young, 1991: Evolution of vortex statistics in two-dimensional turbulence. *Phys. Rev. Lett.* **66**, 2735-2737.

Clercx, H.J.H., and G.J.F. van Heijst, 2009: Two-dimensional Navier-Stokes turbulence in bounded domains. *Appl. Mech. Rev.*, **62**, 020802-1 to -23.

Danilov, S.D., and D. Gurarie, 2000: Quasi-two-dimensional turbulence. *Uspekhi Fizicheskikh Nauk* **170**, 921-968.

Dritschel, D.G., R.K. Scott, C. Macaskill, G.A. Gottwald, and C.V. Tran, 2008: Unified scaling theory for vortex dynamics in two-dimensional turbulence. *Phys. Rev. Lett.* **101**, 094501 – 1-4.

Fu, L.L., 1983: Recent progress in the application of satellite altimetry to observing the mesoscale variability and general circulation of the oceans. *Rev. Geophys. Space Phys.* **21**, 1657-1666.

Kraichnan, R.H., 1967: Inertial ranges in two-dimensional turbulence. *Physics Fluids* **10**, 1417-1423.

LaCasce, J.H., 2008: Statistics from Lagrangian observations. *Prog. Oceanography* **77**, 1-29.

LaCasce, J.H., 2009: The vortex merger rate in freely decaying, two-dimensional turbulence. *Phys. Fluids* **20**, 085102 1-14.

LaCasce, J.H., 2010: Relative displacement PDFs from balloons and drifters. *J. Marine Res.* **60**, 433-457.

Ladyzhenskaya, O., 1969: *The Mathematical Theory of Viscous Incompressible Flows*, Gordon and Breach.

Lesieur, M., 1997: *Turbulence in Fluids*, Klewar.

Lilly, D.K., 1989: Two-dimensional turbulence generated by energy sources at two scales. *J. Atmos. Sci.* **46**, 2026-2030.

Lions, J.-L., and G. Prodi, 1959: "Un theoreme dexistence et unicite dans les equations de Navier-Stokes en dimension 2. *COMPTES RENDUS HEBDOMADAIRES DES SEANCES DE L ACADEMIE DES SCIENCES* **248**, 3519-3521.

McWilliams, J.C., 1984: The emergence of isolated, coherent vortices in turbulent flow. *J. Fluid Mech.* **146**, 21-43.

McWilliams, J.C., 1990: A demonstration of the suppression of turbulent cascades by coherent vortices in two-dimensional turbulence. *Phys. Fluids A* **2**, 547-552.

McWilliams, J.C., 1991: Geostrophic vortices. In: *Nonlinear Topics in Ocean Physics: Proceedings of the International School of Physics "Enrico Fermi"*, Course 109, A.R. Osborne, ed., North-Holland, Elsevier Science Publishers B.V., Amsterdam, 5-50.

McWilliams, J.C. [with unpublished contributions from A. Bracco, X. Capet, J.-P. Laval, M.J. Molemaker, and P.P Sullivan], 2007: Extreme events in geophysical turbulence and waves: What populates the tails of the distribution functions? In: *'Aha Huliko'a Proceedings: 2007*, P. Muller, ed., U. Hawaii, Honolulu, 73-80.

Melander, M.V., N.J. Zabusky, and J.C. McWilliams, 1987: Asymmetric vortex merger in two-dimensions: Which vortex is "victorious"? *Phys. Fluids* **30**, 2610-2612.

Morel, P., and M. Larcheveque, 1974: Relative dispersion of constant-level balloons in the 200 mb general circulation. *J. Atmos. Sci.* **31**, 2189-2196.

Nastrom, G.D., and K.S. Gage, 1985: A climatology of atmospheric wavenumber spectra of wind and temperature observed by commercial aircraft. *J. Atmos. Sci.* **42**, 950-960.

Provenzale, A., A. Babiano, and B. Villone, 1995: Single-particle trajectories in two-dimensional turbulence. *Chaos, Solitons, and Fractals*, 2055-2071.

Weiss, J.B., and J.C. McWilliams, 1993: Temporal scaling behavior of decaying two-dimensional turbulence. *Phys. Fluids A* **5**, 608-621.

Appendix: 2D Vortex Dynamics

Much of the interest in coherent vortices is their role as discrete dynamical elements that collectively yield turbulent behaviors (*i.e.,* the hypothesis of dynamical control). A scientific program

for understanding and calculating turbulence is to identify the important processes for vortex dynamics (this Appendix) and then to use a population of vortices as a basis set for turbulent system dynamics (Sec. 3). The terminology used in this section is only partly explained, and the reader should refer to other sources on geophysical fluid dynamics for fuller explanations.

Individual coherent vortices are nonlinear *stationary states* of the inviscid dynamics. The most common such state is an axisymmetric vortex, with

$$\mathbf{u} \cdot \nabla \zeta \; = \; J[\psi, \zeta] \; = \; 0, \tag{37}$$

and Rayleigh's necessary condition for the instability of a symmetric, 2D flow, *viz.,* the vorticity gradient must change sign within the domain, favors the vorticity monopoles with $\zeta(r)$ monotonically decreasing from the central extremum. There are also other stationary states with a vanishing advection operator in some simple reference frame (*e.g.,* oscillatory $\zeta(r)$, dipoles (modons), tripoles, *etc.*), but none of these have the robustness to perturbations of a $\zeta(r)$ monopole. (One of the major reasons why the coherent structures behave so differently in 2D and 3D homogeneous turbulence is that there are no spatially local, inviscid stationary states in 3D.)

Coherent vortices emerge from complex antecedent conditions or forcing by a dissipative evolution towards a stable, stationary state. For a vorticity monopole, this process is called *axisymmetrization*. The principle argument for it is one of inevitability: there is no other type of localized stationary state with vorticity of a single sign for the flow to evolve towards and escape the nonlinear cascade to enstrophy dissipation. This argument can also be extended to explain the occurrence of the merger interaction of close, like-sign vortices: when the vortices are well separated, like-sign vortices can be a co-rotating stationary state (as with 2 point vortices). But, once they are close enough together, within a distance between centers (*e.g.,* a critical distance, $D_{cr} \approx 3.2R$ for two equal vortices with mean radius R), there are no longer any co-rotating, 2-center stationary states available, and so the flow must evolve to a single-center (*i.e.,* merged) state. The merger interaction involves entwining of the initially distinct vortex cores around each other while casting off vortex filaments that are stretched out until enstrophy dissipation occurs (4). This like-sign vortex pair interaction is in contrast to a close opposite-sign pair, for which the modon stationary state exits, again as with 2 point vortices.

The simplest dynamical system (based on an assumption of a singularized vorticity distribution) that predicts the merger threshold is the *elliptical moment model* (Melander *et al.*, 1987), which is a generalization of the point-vortex model that also represents elliptical deformations of the core vorticity region; outside the threshold separation distance, the moment model has a stationary state of two co-rotating, deformed, like-sign vortices, but inside the threshold the separation distance tends to zero, and the vortex ellipticity tends to infinity with time. The moment model also accounts for the robustness of coherent vortices in the stain field of the flow as a whole.

In a uniform strain field, an elliptically deformed vortex is a stationary solution as long as the ζ amplitude is large enough compared to the background strain rate; otherwise, the vortex will continue to elongate without limit in time. This illustrates another common vortex interaction in 2D turbulence: a weak vortex, of either sign, may be elongated towards irreversible dissipation within the strain field around a stronger vortex, before it is either advected away or brought to merger. This provides a mechanism whereby a population with many weak vortices may evolve towards a distribution with fewer ones (*viz.,* the scaling solution below).

Finally, since an isolated vortex filament is unstable to roll up into new vortices with a size comparable to the filament width, secondary vortex generation may occur if the filaments gener-

ated through vortex interactions are advected outside the elongating and stabilizing influence of the primary vortices; however, turbulent solutions indicate this secondary generation process is relatively rare.